2010 IEEE International Conference on Robotics and Automation
Anchorage Convention District
May 3-8, 2010, Anchorage, Alaska, USA

Anti-Windup Design for Trajectory Tracking of a Parallel Robot – an Holistic Approach

Frank Wobbe, Dang Hung Nguyen and Walter Schumacher

Abstract— **This paper presents motion control concepts on parallel robots with explicit focus on anti-windup-design and trajectory-tracking. Starting from modeling and exact feedback linearization, a cascade control is designed. Improvements to control laws with respect to input-saturations are derived by using concepts of anti-windup compensation. A multiple-axis anti-windup-control is presented, guaranteeing tracking in case of input-saturation. Control schemes are implemented on a planar parallel manipulator for performance evaluation of high dynamic operation. Efficiency of control is highlighted with respect to trajectory tracking i. e. Cartesian distortion. All concepts are derived in a formal way guaranteeing manipulator-independent results and transferability.**

I. INTRODUCTION

Robot structures based on closed kinematic chains gain more and more acceptance in industrial application, as they have proven to be a promising alternative to those based on serial chains. The feature of many of these so called parallel kinematic structures is especially of great interest for the design of robots for high speed handling and assembly tasks as they allow for the drives to be fixed in the base [1]. Design concepts featuring low moved masses are enabled and thus they outperform their serial counterparts by high dynamic performance combined with precision and stiffness. Shorter cycle times in assembly tasks can be achieved. Therefore, the design of control concepts has to address these features in order to maximize the performance of the robot. Due to the non-linearities of the manipulators, a model-based control architecture is essential to ensure precise trajectory tracking. Among centralized control schemes inverse dynamics control is a common approach to control manipulators [2]. The controllers for each axis are designed independently within a linear framework. Thus, the drive controller is used to encapsulate the dynamics of the manipulator in a fixed coordinate system. The design of the subordinated drive-controller is based on a torque driven interface to the inverters at the bottom layer and provides a uniform trajectory interface to the top layer, specified by position, velocity and acceleration $\{\mathbf{x}_{ref}, \dot{\mathbf{x}}_{ref}, \ddot{\mathbf{x}}_{ref}\}$ in the base-frame of the robot. This concept ensures hybrid control within the task-frame formalism [3], [4], and thus, the presented controllers do not restrict the manipulator to position control, see [5]. As actuators are constrained, nonlinear effects have to be taken into account in design to prevent windup effects when using integral control action [6]. Different anti-windup-compensator schemes can be applied. In multiple-axis control special attention has to be paid to trajectory tracking to prevent a distortion of the trajectory [7] and preserving directionality [8]. This paper presents the design of anti-windup compensation with extension to a special frame, that guarantees tracking without modification of the reference trajectory (which normally is applied, see [9]) – this solution of the directionality problem circumvents the use of a reference shaping filter. The paper is organized as follows. First, the derivation of the robots model based on the Jacobian matrices and discrete modelling is presented. The next section introduces the classical control structures based on exact feedback linearization. Taking nonlinearities, i. e. saturation of actuators into account, an anti-windup-compensation scheme is presented which is enhanced to the multiple axes case guaranteeing trajectory tracking. The strategies are verified and implemented on the planar parallel manipulator FIVEBAR, see Fig. 1. The results and performance of the different strategies are presented and discussed within the last sections.

Fig. 1. Planar parallel manipulator FIVEBAR

II. MODELLING OF THE MANIPULATOR

Different methods of modelling parallel robots have been proposed in literature: On the one hand approaches based on the Newton-Euler method can be found, on the other hand the Lagrangian method is common [10], [11]. From the latter group the formulation of Lagrange-D'Alembert [12], [13] in combination with discrete modelling has proven to be computationally efficient for realtime-control [14]. The core idea consists of the use of Jacobians for discrete modelling and is presented in short.

Frank Wobbe, Dang Hung Nguyen and Walter Schumacher are with the INSTITUTE OF CONTROL ENGINEERING, TECHNISCHE UNIVERSITÄT BRAUNSCHWEIG, 38106 Braunschweig, Germany wobbe@ifr.ing.tu-bs.de

A. Discrete Modelling – Manipulator Jacobian and Differential Equations

Discrete modeling of parallel structures can be subdivided into two parts: Derivation of the manipulators Jacobian $\mathbf{J}$ and calculation of differential equations.

The first step relies on principles of kineto-static, representing differential kinematic and static relation as $\dot{\mathbf{x}} = \mathbf{J}\dot{\mathbf{q}} \leftrightarrow \boldsymbol{\tau} = \mathbf{J}^{\mathrm{T}}\mathbf{f}$. The kinematic structure of the parallel manipulator is deduced into n tree structures by cutting open kinematic loops at the endeffector E. Assuming all passive joints without elasticities, connected links to the endeffector do transmit only longitudinal forces. Computing internal link-forces

$$\begin{aligned}\begin{bmatrix} f_{p_1} & \dots & f_{p_n} \end{bmatrix}^{\mathrm{T}} &= \begin{bmatrix} S_1 & \dots & S_n \end{bmatrix}^{-1} \mathbf{f}_{ext} \\ &=: \mathbf{S}^{-1}\mathbf{f}_{ext}\end{aligned} \tag{1}$$

with an external force $\mathbf{f}_{ext}$ applied and using Jacobians of passive joints $\mathbf{J}_{p_i}$ with $i \in [1, \dots, n]$ leads to the Jacobian of parallel manipulator:

$$\begin{aligned}\mathbf{G}^{+} &= \mathrm{diag}\{\mathbf{J}_{p_1}, \dots, \mathbf{J}_{p_n}\}^{\mathrm{T}} \mathrm{diag}\{S_1, \dots, S_n\}\mathbf{S}^{-1} \\ &= \mathbf{J}_E^{\mathrm{T}} = \mathbf{J}^{\mathrm{T}}.\end{aligned} \tag{2}$$

Here, $\mathbf{G}^{+} = \mathbf{G}^{-1} = \mathbf{J}^{\mathrm{T}}$ holds a relation between Jacobian of serial and parallel manipulators (joint space: $\dot{\mathbf{x}} = \mathbf{J}\dot{\mathbf{q}}$, operational space: $\mathbf{f} = \mathbf{G}\boldsymbol{\tau}$, duality of Jacobians, see [10]). As pointed out and discussed in detail in [15], the Jacobian of the endeffector along with the derivatives of passive joints can be deduced in a single step.

In a second step the differential equations can be calculated by using already derived Jacobians and applying Lagrange-D'Alembert-Formulation (Lagrange-Type II):

$$\frac{\mathrm{d}}{\mathrm{d}t}\left(\frac{\partial L}{\partial \dot{\mathbf{q}}}\right) - \frac{\partial L}{\partial \mathbf{q}} = \boldsymbol{\tau} + \mathbf{J}^{\mathrm{T}}\mathbf{f}_{ext} \tag{3}$$

with $L = T - V$ representing the Lagrange-function, T kinetic energy, V potential energy, $\mathbf{q}$ vector of joint space variables, $\boldsymbol{\tau}$ being actuator torques and external forces $\mathbf{f}_{ext}$ which are applied on the endeffector. Energy functions can be computed as:

$$T = \frac{1}{2}\dot{\mathbf{q}}^{\mathrm{T}}\mathbf{M}_q(\mathbf{q})\,\dot{\mathbf{q}}, \qquad V = \int_{\mathbf{q}_0}^{\mathbf{q}} \boldsymbol{\eta}_q(\mathbf{q})\,\mathrm{d}\mathbf{q} \tag{4}$$

which leads to a differential equation in joint space coordinates:

$$\mathbf{M}_q(\mathbf{q})\,\ddot{\mathbf{q}} + \mathbf{C}_q(\dot{\mathbf{q}}, \mathbf{q})\,\dot{\mathbf{q}} + \boldsymbol{\eta}_q(\mathbf{q}) = \boldsymbol{\tau} + \mathbf{J}^{\mathrm{T}}\mathbf{f}_{ext} \tag{5a}$$

In the case of planar structures each link can be modelled by discrete point masses m_i without modifying dynamical behaviour [16]. Using this discrete inertia-distribution allows a simple algorithm for deducing matrices:

$$\begin{aligned}\mathbf{M}_q &= \sum_i m_i \mathbf{J}_i^{\mathrm{T}}\mathbf{J}_i + \mathrm{diag}\{I_m, I_m\}, \\ \mathbf{C}_q &= \frac{\partial \mathbf{M}_q}{\partial t} - \frac{1}{2}\frac{\partial\left(\dot{\mathbf{q}}^{\mathrm{T}}\mathbf{M}_q\right)}{\partial \mathbf{q}}, \\ \boldsymbol{\eta}_q &= \sum_i m_i \mathbf{J}_i^{\mathrm{T}}\mathbf{g},\end{aligned} \tag{5b}$$

with $\mathbf{g}$ being vector of gravitation. Hereby all Jacobians $\mathbf{J}_i$ (representing differential kinematics in location of point-mass m_i) can be described as a linear combination of endeffector- and passive-joints-Jacobians, as deduced in eq. (2). The choice of Coriolis-matrix is not unique: Using Christoffel-symbols and following the notation of [17] and [18] with discussion in [19] leads to

$$\begin{aligned}\mathbf{C} = \frac{1}{2}\left\{\left(\dot{\mathbf{q}}^{\mathrm{T}} \otimes \mathbf{I}_n\right) - \left(\mathbf{I}_n \otimes \dot{\mathbf{q}}^{\mathrm{T}}\right)\right\}\frac{\partial \mathbf{M}_q}{\partial \mathbf{q}} \\ + \frac{1}{2}\left\{\left(\mathbf{I}_n \otimes \dot{\mathbf{q}}^{\mathrm{T}}\right)\frac{\partial \mathbf{M}_q}{\partial \mathbf{q}}\right\}^{\mathrm{T}},\end{aligned} \tag{6}$$

where $\otimes$ denotes the Kronecker-product. By eq. (6) the skew-symmetry of $\dot{\mathbf{M}}_{\mathbf{q}} - 2\mathbf{C}_{\mathbf{q}}$ is featured, e. g.

$$\mathbf{w}^{\mathrm{T}}\left(\dot{\mathbf{M}}_q - 2\mathbf{C}_q\right)\mathbf{w} = \mathbf{0}, \qquad \mathbf{w} \in \mathbb{R}^{(n\times 1)}, \tag{7}$$

which simplifies their usage for control algorithms [2]. This formalism can be used for planar structures without loss of generality and is extensible to general ones.
The differential equation of the parallel manipulator in operational space computes as:

$$\mathbf{M}_x(\mathbf{q})\,\ddot{\mathbf{x}} + \mathbf{C}_x(\dot{\mathbf{q}}, \mathbf{q})\,\dot{\mathbf{x}} + \boldsymbol{\eta}_x(\mathbf{q}) = \mathbf{G}\boldsymbol{\tau} + \mathbf{f}_{ext} \tag{8a}$$

with:

$$\begin{aligned}\mathbf{M}_x &= \mathbf{J}^{-\mathrm{T}}\mathbf{M}_q\mathbf{J}^{-1} = \mathbf{G}\mathbf{M}_q\mathbf{G}^{\mathrm{T}}, \\ \mathbf{C}_x &= \mathbf{J}^{-\mathrm{T}}\left(\mathbf{C}_q\mathbf{J}^{-1} + \mathbf{M}_q\dot{\widehat{\mathbf{J}^{-1}}}\right) \\ &= \mathbf{G}\left(\mathbf{C}_q\mathbf{G}^{\mathrm{T}} + \mathbf{M}_q\dot{\mathbf{G}}^{\mathrm{T}}\right), \\ \boldsymbol{\eta}_x &= \mathbf{J}^{-\mathrm{T}}\boldsymbol{\eta}_q = \mathbf{G}\boldsymbol{\eta}_q,\end{aligned} \tag{8b}$$

where eq. (7) still holds. Matrices still depend on joint space variables which is advantageous, because measurements are sampled in joint space. Thus, it circumvents the solution of the direct kinematic problem (DKP), for which an analytical solution exists only in special cases and not in general for parallel kinematics.

B. The manipulator FIVEBAR

For experimental setup a planar parallel structure with two degrees of freedom, named FIVEBAR (see Fig. 1), is used. The endeffector of the manipulator is connected to the drives by two independent kinematic chains. To reduce the weight of the moved masses, cranks and rods of the manipulator are made of carbon fiber. Hence the FIVEBAR is well-suited for highspeed operation with a maximum velocity $v = 5\,\mathrm{m/s}$ and acceleration $a = 70\,\mathrm{m/s^2}$ in Cartesian

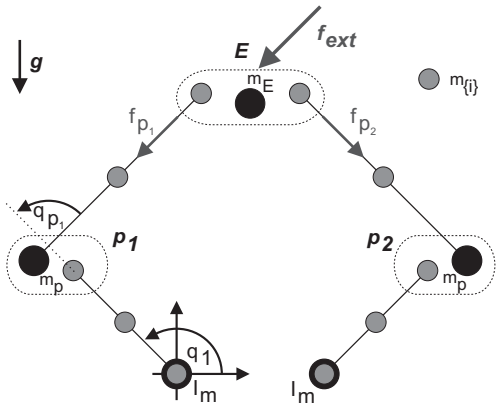

Fig. 2. Discrete modell of FIVEBAR

space. The control systems bases on a PC running QNX as operating system which is linked to the inverters via IEEE 1396 FireWire. Hence a short cycle time and sufficient bandwidth for control purposes is ensured.

Discrete modelling as given in subsection II-A is applied to deduce the differential dynamics equations. The discrete mass-distribution, inherent to discrete modelling, is depicted in Fig. 2.

III. CONTROL CONCEPTS

In the context of the overall system the drive controller encapsulates the dynamics of the manipulator in a fixed coordinate system. A model-based control is set up that is enhanced by an anti-windup-scheme. In the following the explicit specification of matrix-dependencies is skipped for keeping simplicity.

A. Inverse Dynamics Feedback and Cascade Control

Classical linear control concepts can be applied, if linearization techniques are used. Here we use inverse dynamics feedback control which acts as exact feedback linearization. The model derived in subsection II-A is used to set up an external reference input $\mathbf{u}$, that renders the closed loop dynamical behavior to a set of decoupled double integrators in Cartesian space [20], by applying

$$\boldsymbol{\tau} = \mathbf{G}^{-1}\widehat{\mathbf{M}}_x\mathbf{u} + \mathbf{G}^{-1}\boldsymbol{\xi}_x, \quad \boldsymbol{\xi}_x = \widehat{\mathbf{C}}_x\dot{\mathbf{x}} + \widehat{\boldsymbol{\eta}}_x, \tag{9}$$

see eq. (8a). Note, that the existence of an analytical solution of the DKP for the manipulator FIVEBAR has been utilized. For simplicity, linearization neglects the dynamic effects of the inverters because of the large difference between electrical and mechanical time constants. Taking the delay of the inverter, denoted by T_{el}, into account yields

$$u_i = T_{el}x_i^{(3)} + x_i^{(2)}, \quad i \in \{1, \ldots, n\}, \tag{10}$$

as dynamic behaviour of the linearized subsystems. Based on the linearized subsystem given by eq. (10) a cascaded control scheme is designed as depicted in Fig. 3 with transfer functions

$$K_{vel}(s) = V_1\frac{T_I s + 1}{T_I s}, \quad K_{pos}(s) = V_2\frac{T_R s + 1}{T_L s + 1} \tag{11}$$

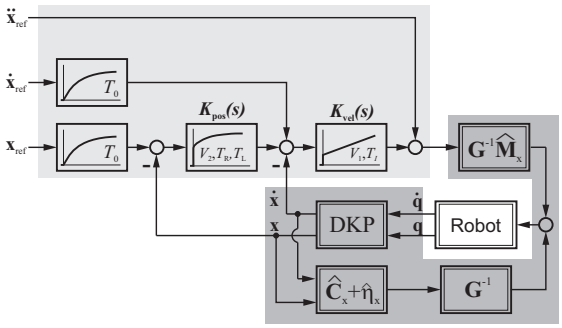

Fig. 3. Cascade Control

for axes' velocity and position controller, respectively. The inner loop is parametrized via symmetrical optimum (see [21]), which ensures stability in the presence of model uncertainties. In the outer loop a PTD-controller is preferred to the classical P-controller to suppress the inherent overshoot of the velocity controller. For disturbance reduction and efficient feed forward dynamics, parameters are determined by an optimization. Comparing the denominator of the closed loop dynamics with a model function and placing all poles except one complex pair onto the real axis allows the extraction of damping D as an independent parameter. Using an integral criterion for minimizing the disturbance step response yields optimized parameters as

$$\begin{aligned} V_1 &= \frac{5D^2+1}{16D^2T_{el}}, & T_I &= \frac{4T_{el}\left(5D^2+1\right)}{1+2D^2}, \\ V_2 &= \frac{1}{4T_{el}\left(1+2D^2\right)}, & T_R &= 4T_{el}, \qquad T_L = T_I \end{aligned} \tag{12}$$

and ensures tracking in Cartesian space. For details of design consider [22] and [23] – for a comparison to other control schemes with respect to performance we refer to [24].

B. Anti-Windup Control

In general, actuators are constrained by their output and bandwidth. While the later one is taken into account during controller design in subsection III-A, additional techniques have to be applied for dealing with input-saturation to prevent tracking errors and – more crucial – instability of closed loop control.

Anti-windup schemes are quite common in case of coping with input saturations [6]. They can be divided into two major groups – observer based anti-windup (OBSAWC) [25] and general linear anti-windup compensators (GLAWC) [7], [26]. We here use GLAWC, whose classical design is depicted in Fig. 4 and considers plant and controller windup. During the design process two system dynamics are of interest. On the one hand windup is measured by compairing the system output $\mathbf{y}$ with saturating actuators to that of a linear system $\mathbf{y}_l$, represented by a system dynamic $\mathbf{H}_\delta$:

$$\begin{aligned} \mathbf{y}_\delta &= \mathbf{y} - \mathbf{y}_l = \mathbf{H}_\delta\left(\mathbf{v} - \mathbf{u}\right) = \mathbf{H}_\delta\boldsymbol{\delta} \\ \mathbf{y} &= \mathbf{y}_l + \mathbf{H}_\delta\boldsymbol{\delta}. \end{aligned} \tag{13a}$$

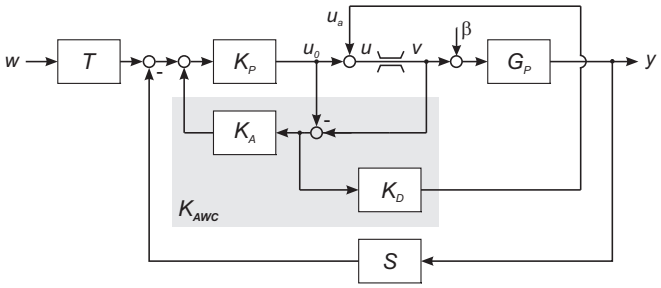

Fig. 4. Anti-Windup-Control

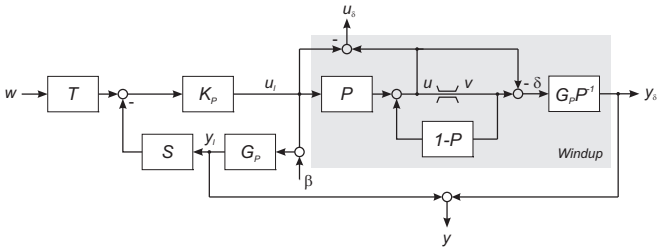

Fig. 5. Windup-dynamics

On the other hand stability properties are covered by the use of describing function analysis (harmonic balance analysis) [27], which uses the loop transfer function $\mathbf{L}_v$ around the nonlinearity, i. e. the saturation:

$$\mathbf{u} = \mathbf{L}_v\mathbf{v} + \mathbf{K}\left(\mathbf{T}\mathbf{w} - \mathbf{G}_P\mathbf{S}\boldsymbol{\beta}\right), \qquad \mathbf{v} = \mathrm{sat}(\mathbf{u}). \tag{13b}$$

With respect to anti-windup design in Fig. 4 the dynamics result in:

$$\begin{aligned}\mathbf{L}_v &= \mathbf{I} - \left(\mathbf{I} - \mathbf{K}_D\right)\left(\mathbf{I} + \mathbf{K}_P\mathbf{K}_A\right)^{-1}\left(\mathbf{I} + \mathbf{K}_P\mathbf{S}\mathbf{G}_P\right)\\ \mathbf{H}_\delta &= \mathbf{G}_P\left(\mathbf{I} + \mathbf{K}_P\mathbf{S}\mathbf{G}_P\right)^{-1}\left(\mathbf{I} + \mathbf{K}_P\mathbf{K}_A\right)\left(\mathbf{I} - \mathbf{K}_D\right)^{-1}\\ \mathbf{K} &= \left(\mathbf{I} - \mathbf{K}_D\right)\left(\mathbf{I} + \mathbf{K}_P\mathbf{K}_A\right)^{-1}\mathbf{K}_P. \end{aligned} \tag{13c}$$

It can be seen that

$$\mathbf{P} := \left(\mathbf{I} - \mathbf{K}_D\right)\left(\mathbf{I} + \mathbf{K}_P\mathbf{K}_A\right)^{-1}\left(\mathbf{I} + \mathbf{K}_P\mathbf{S}\mathbf{G}_P\right) \tag{13d}$$

can be denoted as a common parameter for both dynamics and will be used for the design. The effects of windup represented by eq. (13) can be seen in Fig. 5. Using appropriate design for $\mathbf{K}_A$ and $\mathbf{K}_D$ copes with windup and thus reduces tracking errors (represented by dynamics of $\mathbf{H}_\delta$) and instability (see $\mathbf{L}_v$) in case of input saturation.

IV. Parametric Anti-Windup Design and Implementation

Parametric design bases on eq. (13) and design of inner cascade, i. e. $G_P = \frac{1}{(T_{el}s+1)s}$, $K_P = K_{vel}(s)$, $S = 1$, $T = 1$, $y = \dot{x}$ for each d.o.f., see eq. (11) and eq. (12). Hence, parametric design can be handled for each axis (i. e. for each d.o.f.) individually or in an holistic approach for the overall system dynamic. Here the design of the outer cascade remains as in subsection III-A as controllers used for position control here do not rely on integral action.

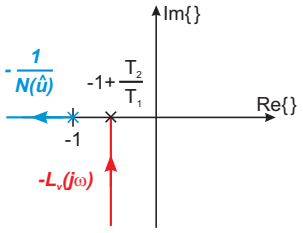

Fig. 6. Nyquist plot / harmonic balance of input saturation and system dynamics

A. Single-Axis Anti-Windup Control

The core idea consists of finding a system dynamic H_δ that guarantees tracking with linear error dynamics in case of saturation on the one hand and stability of windup dynamics L_v on the other hand. As a result a bounded difference in velocity, i. e. $\dot{x}_\delta \leq k\delta$, with k bounded, can be expected. These specifications can be matched by parametric design

$$\begin{aligned} P &= \frac{T_2 s + 1}{T_1 s}, \qquad 0 < T_2 < T_1,\\ H_\delta &= \frac{T_1}{\left(T_{el}s + 1\right)\left(T_2 s + 1\right)},\\ L_v &= -\frac{\left(T_2 - T_1\right)s + 1}{T_1 s}. \end{aligned} \tag{14}$$

Denoting

$$N(\hat{u}) = \begin{cases} 1 & , 0 \leq \hat{u} \leq u_{\max} \\ \frac{2}{\pi}\left[\arcsin\left(\frac{u_{\max}}{\hat{u}}\right) + \frac{u_{\max}}{\hat{u}}\sqrt{1 - \left(\frac{u_{\max}}{\hat{u}}\right)^2}\right] & , \hat{u} > u_{\max} \end{cases} \tag{15}$$

as describing function for saturation and using the harmonic balance equation

$$-L_v(\mathrm{j}\omega)N(\hat{u}) + 1 = 0, \tag{16}$$

stability is verified via Nyquist plot as depicted in Fig. 6. Hence, stability in presence of input saturation is ensured. Taking the $\mathcal{H}_\infty$ and $\mathcal{L}_1$ norm with the peak-to-peak gain

$$\|\dot{x}_\delta\|_\infty \leq \|H_\delta\|_1\|\delta\|_\infty = T_1\|\delta\|_\infty \tag{17}$$

into account (see Fig. 5), it can be seen that the velocity difference $\dot{x}_\delta$ is bounded and proportional to δ for the stationary case.

B. Multiple-Axis Anti-Windup Control

In robotics and other multiple axis-control applications a fully specified C^2-continuous reference trajectory $\{\mathbf{x}_{ref}(t), \dot{\mathbf{x}}_{ref}(t), \ddot{\mathbf{x}}_{ref}(t)\}$ with $\mathbf{x}_{ref} = \left[x_{1,ref}, \ldots x_{n,ref}\right]^\mathsf{T}$ is quite common. In case of an output error in a single axis, a distortion of the path in operational space is inevitable, as parametric design in the former subsection has not taken errors in other axes into account yet – the saturation may not preserve directionality anymore, see [8]. A special design of anti-windup overcomes this drawback. The core idea consist of taking the trajectory, i. e. the coupling $\gamma_{(i,j)}$ of axes i and

j, into account and relating it to the position error in these axes:

$$\gamma_{(i,j)} = \frac{\dot{x}_{i,ref}}{\dot{x}_{j,ref}} \stackrel{!}{=} \frac{\Delta x_i}{\Delta x_j} = \frac{\int \mathbf{e}_i^{\mathrm{T}} \mathbf{H}_\delta * \boldsymbol{\delta} \mathrm{d}t}{\int \mathbf{e}_j^{\mathrm{T}} \mathbf{H}_\delta * \boldsymbol{\delta} \mathrm{d}t}, \quad i \neq j, \tag{18}$$

where $\mathbf{e}_k$ represents the unit vector of axis k. Let $\gamma_{(i,i)} = 0$ and $\gamma_{(i,j)}$ be finite, i. e. $\gamma_{(i,j)} = 0$ for $\dot{x}_{j,ref} = 0$, so that $\boldsymbol{\Gamma}$ denotes the corresponding matrix with elements $\gamma_{(i,j)}$[1]. Assuming that input saturation occurs only in one axis k at a time, a solution for parametric design is given by

$$\begin{aligned} \mathbf{P}_k &= \left[\mathbf{I}_n + \mathbf{e}_k^{\mathrm{T}} \otimes (\boldsymbol{\Gamma}\mathbf{e}_k)\right]^{-1} P \\ \mathbf{H}_{\delta_k} &= \left[\mathbf{I}_n + \mathbf{e}_k^{\mathrm{T}} \otimes (\boldsymbol{\Gamma}\mathbf{e}_k)\right] H_\delta \\ \mathbf{L}_{v_k} &= \mathbf{I}_n L_v + \left[\mathbf{e}_k^{\mathrm{T}} \otimes (\boldsymbol{\Gamma}\mathbf{e}_k)\right] P \end{aligned} \tag{19}$$

to fullfill eq. (18). Here, results of parametric design in eq. (14) have been used. The index k indicates that the solution depends on the index of the the saturated axis, i. e. the parametric design is (on-line) adapted to the saturated axis and to trajectory data at each point in time, see eq. (18).

Following the generalized Nyquist criterion as pointed out in [28], [29] stability can be proven by Nyquist plots of eigenvalues $\lambda_{i,\,-\mathbf{L}_{v_k}}(s) := \lambda_i\left\{-\mathbf{L}_{v_k}(s)\right\}$ and the negative inverse describing function $-\frac{1}{N(\hat{u})}$ of the saturation. Parametric design in eq. (19) features that eigenvalues of $\mathbf{L}_{v_k}$ do not change compared to the single axis design in eq. (14):

$$\begin{aligned} \lambda_i\left\{-\mathbf{L}_{v_k}(s)\right\} &= -\lambda_i\left\{\mathbf{I}_n L_v(s) + \left[\mathbf{e}_k^{\mathrm{T}} \otimes (\boldsymbol{\Gamma}\mathbf{e}_k)\right] P(s)\right\} \\ &= \lambda_i\left\{-L_v(s)\right\}. \end{aligned} \tag{20}$$

Moreover, the saturation function consists of n equal saturations for multiple axes control, and thus the corresponding describing function equals the single axis control case, see eq. (15). Hence, the stability analysis for multiple axes reduces to the single axis case, which is given by the Nyquist plot in Fig. 6 – the closed loop control is stable.

The velocity difference $\dot{\mathbf{x}}_\delta$ is bounded

$$\begin{aligned} \|\dot{\mathbf{x}}_\delta\|_\infty &\leq \max_k\{\|\mathbf{H}_{\delta_k}\|_1\}\,\|\boldsymbol{\delta}\|_\infty \\ &= \max_{i,k}\left\{\sqrt{1+\gamma_{(i,k)}^2}\right\} T_1 \|\boldsymbol{\delta}\|_\infty, \end{aligned} \tag{21}$$

because $\gamma_{(i,k)}$ is finite. Here, $\|\mathbf{v}\|_\infty$ denotes the $\mathcal{H}_\infty$ norm of the euclidean norm $|\mathbf{v}|$ of the vector $\mathbf{v}$. Moreover,

$$\dot{\mathbf{x}}_\delta \sim \max_{i,k}\left\{\sqrt{1+\gamma_{(i,k)}^2}\mathbf{e}_k^{\mathrm{T}}\boldsymbol{\delta}\right\} \frac{\dot{\mathbf{x}}_{ref}}{|\dot{\mathbf{x}}_{ref}|} \tag{22}$$

is valid for the stationary case, i. e. the orientation of reference velocity in operational space is retained. Although the position error $\mathbf{x}_\delta$ is unbounded in case of saturation, a bounded distortion $d(t)$ is gained by the parametric design. Distortion here is defined by the distance between the actual position and the reference trajectory:

$$d(t) = \mathrm{dist}\left(\mathbf{x}_{act}(t), \mathbf{x}_{traj}\right), \tag{23}$$

[1] in detail: $\boldsymbol{\Gamma} = \sum_{j=1}^{n}\sum_{i=1}^{n} \gamma_{(i,j)} \mathbf{e}_j^{\mathrm{T}} \otimes \mathbf{e}_i$

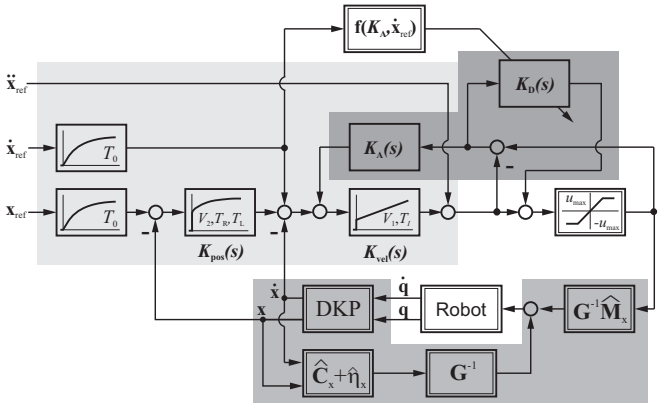

Fig. 7. Overall control scheme

with $\mathbf{x}_{act}(t)$ as actual position of the endeffector in operational space and

$$\mathbf{x}_{traj} = \left\{\mathbf{g} \mid \exists t_l \leq \tau \leq t_{l+1} \in \mathbb{R}^+ : \mathbf{g} = \mathbf{x}_{ref}(\tau)\right\}$$

as the set of all points of the reference trajectory between points t_l and t_{l+1} in time. As a sidenote it can be mentioned that eq. (22) can be used for specification of a maximum contouring error of velocities for safety reasons – the one of position is inapplicable due to possible unboundedness.

C. Overall control scheme

Saturations of actuators within the nonlinear framework demand for variable upper and lower bounds $u_{\max}$ of saturations $\mathrm{sat}_{\mathbf{u}_{\max}}$ within the linear framework. Given a boundary $\boldsymbol{\tau}_{\max}$ as maximum torque applicable to the robot and respecting eq. (9), it follows

$$\mathbf{u}_{\max} = \widehat{\mathbf{M}}_x^{-1}\left(\mathbf{G}\boldsymbol{\tau}_{\max} - \widehat{\mathbf{C}}_x\dot{\mathbf{x}} - \widehat{\boldsymbol{\eta}}_x\right) \tag{24}$$

as boundary of saturations. It may serve as an adaption law or can be used for determination of maximum static boundaries to ensure $\forall t \in \mathbb{R}^+ : \boldsymbol{\tau}(t) \leq \boldsymbol{\tau}_{\max}$. Though boundaries $\mathbf{u}_{\max}$ effect the parameterization of describing function $N(\hat{u})$, its shape is persistant, see eq. (15). Thus, adaption is applicable as long as $u_{\max} > 0$ is valid for each axis, and dynamic of adaption is assumed to be slow compared to the one of control [30]. Furthermore, parametrization of anti-windup compensators given by eq. (13c) can be refined by choosing

$$\begin{aligned} \mathbf{K}_A &= \mathbf{I}K_A \\ \mathbf{K}_{D_k} &= \mathbf{I}K_D + \left[\mathbf{e}_k^{\mathrm{T}} \otimes (\boldsymbol{\Gamma}\mathbf{e}_k)\right](1 - K_D), \end{aligned} \tag{25}$$

with K_A and K_D denoting scalar transfer functions with appropriate parametrization according to eq. (13d) and eq. (14). As $\mathbf{K}_{D_k}$ depends on feedforward values, the principle of gain scheduling [31] is convenient for control, which results in overall control scheme depicted in Fig. 7. The problem of conserving directionality here is solved by parametric design instead of using a reference shaping filter. Thus, trajectory tracking in case of input saturation is ensured without modification of trajectory.

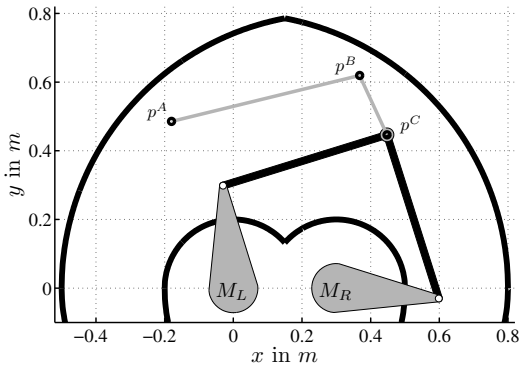

Fig. 8. Workspace and experimental setup of FIVEBAR

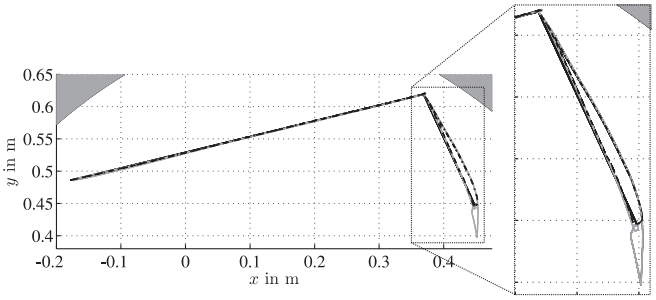

Fig. 9. Trajectory of FIVEBAR: linear (gray solid), single-axis anti-windup (black dash-dotted), multiple-axis anti-windup (black dashed) and linear saturated (gray solid) control.

V. EXPERIMENTAL RESULTS

Controller designed in section III and section IV were experimentally verified on the demonstrator FIVEBAR. Its workspace and the trajectory for all experimental setups is given in Fig. 8. The area of Cartesian distortion Δ_A is defined for benchmarking path-accuracy in operational space by

$$\Delta_A = \sum_i \left| \int_{t_i}^{t_{i+1}} \mathrm{dist}\left(\mathbf{x}_{act}(t), \mathbf{x}^*_{traj}\right) \dot{\mathbf{x}}^{\mathrm{T}}_{act}(t) \frac{\dot{\mathbf{x}}_{proj}(t)}{|\dot{\mathbf{x}}_{proj}(t)|} \mathrm{d}t \right|,$$

where t_i marks the start time of trajectory i and $\mathbf{x}_{proj}(t)$ denotes the projected point of actual position $\mathbf{x}_{act}$ onto the virtual extrapolated reference trajectory $\mathbf{x}^*_{traj}$. It is a measure of the absolute size of distortion-areas and thus indicates accuracy of the endeffector path with respect to the reference trajectory.

In terms of distortion over time its maximum value $d_{\max} = \max\{\mathrm{dist}\left(\mathbf{x}_{act}(t), \mathbf{x}_{traj}\right)\}$ is another important indicator for performance with respect to system dynamics. It is an integral benchmark for eq. (22), as it indicates overshooting of trajectory in operational space and thus gauges an error in orientation of velocity.

To determine the level of saturation, the maximum values of absolute velocity error $|\Delta\dot{\mathbf{x}}|_{\max} = |\dot{\mathbf{x}}_{ref} - \dot{\mathbf{x}}_{act}|_{\max}$ and input saturation $|\boldsymbol{\delta}|_{\max}$ are taken as reference.
Plots of experimental results are given in Fig. 9 - Fig. 13 and will be discussed in the following. The trajectory of FIVEBAR consists of two parts and is depicted in Fig. 9. It can be seen that the second part of the trajectory is of particular importance for benchmarking and will be paid special attention. Corresponding time plots are presented in Fig. 10, where the two parts of trajectory are indicated by a break in the time-axis. In comparing the linear case (i. e. no saturation, see subfigures with index (a)) to the saturated one (i. e. with windup effects, see subfigures with index (b)) the effects of windup on the path of the endeffector can be noted. Not only the contouring error increases, but also the distortion – the reference trajectory cannot be followed on time. The saturation limits are set to $\pm 25\ \mathrm{m/s^2}$ within the linear framework. Using the presented multiple-axis anti-windup scheme (see subfigures with index (c)) the effects of windup are reduced. Although a contouring error is still present, the actual postion does not overshoot the reference trajectory anymore. Furthermore, the difference of saturated and unsaturated actuating variable, denoted by δ, is cut down as shown in Fig. 11. However, cycle times increase as the excecution time of a skill primitive lengthens. Comparing the actuating variables of the linear to the anti-windup control concept only narrow differences in characteristics are visible for the part where no saturation occurs – the difference in actuating variables at the end of the second part of the trajectory is not stationary. When the actuating variable saturates, an influence on the other axis is reflected by differences in behavior over time. A more detailed study, revealing impacts on performance, is given by the distortion over time plot in Fig. 12. The anti-windup scheme features a lesser maximum of distortion compared to the linear control scheme, which is a positive side-effect of the design of the velocity-cascade via symmetrical optimum, featuring the property that the integral of velocity error tends to zero. Thus, overshooting is lesser in case of a bounded output of the PI-controller. Analysis with respect to the saturated case (b) in contrast unveils a massive distortion due to the vectorial error of velocities $\Delta\dot{\mathbf{x}}$ given in Fig. 13. They are normalized to the maximum norm of the vectorial error in the saturated case (b). To retain orientation of reference trajectory, occurring errors have to fullfill eq. (18), which is represented by the dashed line. I. e. velocity errors and reference trajectory have to adopt a common orientation. While this is valid for the linear and the anti-windup control scheme, errors perpendicular to the reference trajectory can be noted in case of linear control with saturation, resulting in a large distortion, consequently.

For a quantitative comparison all control concepts are faced to each other in Fig. 14, where each value of interest has been normalized to the corresponding value in case of linear control with saturation (b). The control scheme with anti-windup compensators designed for each single axis independently is additionally listed for completeness. Though the maximum absolute velocity error is large for the anti-windup case compared to the linear control case, the distortion is kept in the same range, proving the performance of anti-windup design in line with trajectory tracking.

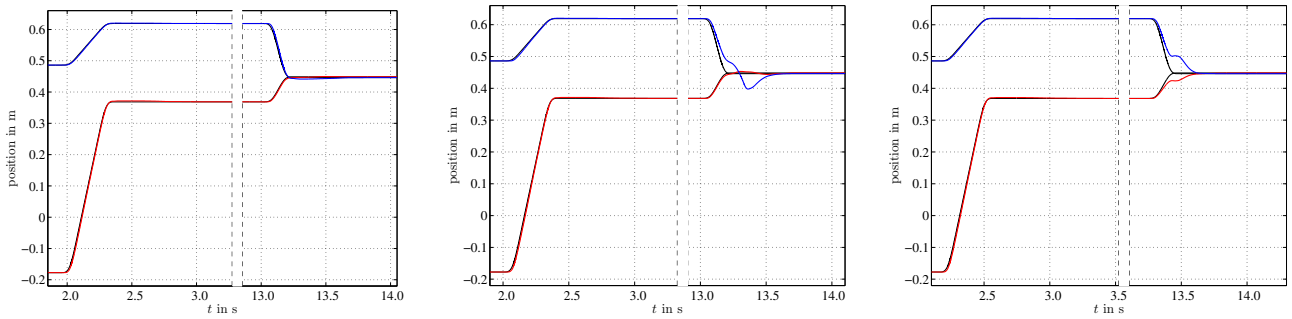

(a) linear control (b) linear control with saturation (c) multiple-axis anti-windup control

Fig. 10. Trajectory tracking: reference (black), actual x-position (red), actual y-position (blue).

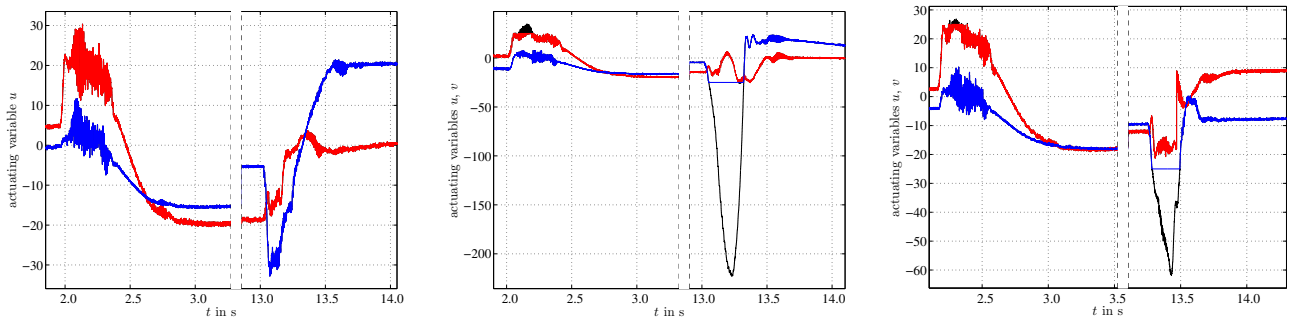

(a) linear control (b) linear control with saturation (c) multiple-axis anti-windup control

Fig. 11. Actuating variables: input to saturation (black), output of saturation in x-axis (red), output of saturation in y-axis (blue).

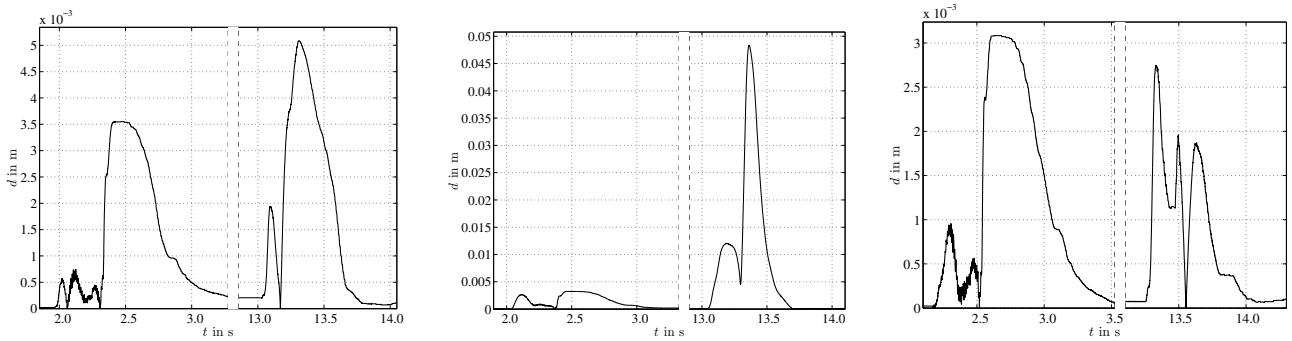

(a) linear control (b) linear control with saturation (c) multiple-axis anti-windup control

Fig. 12. Distortion as distance between the actual position and the reference trajectory in Cartesian space

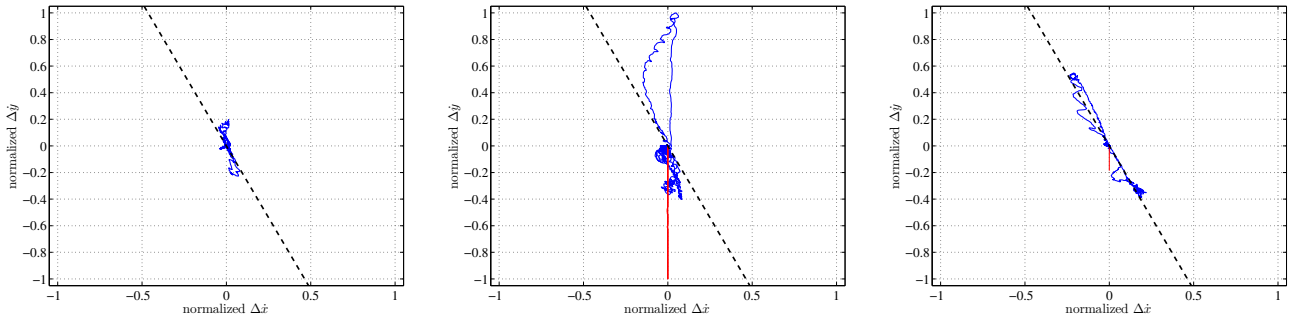

(a) linear control (b) linear control with saturation (c) multiple-axis anti-windup control

Fig. 13. Vectorial velocity errors during the second part of trajectory as locus plot (normalized to the linear control with saturation case): orientation of trajectory (black dashed), vector of velocity error parameterized by time (blue solid) and difference of input to and output of saturation with respect to axes as vectoriel plot (red).

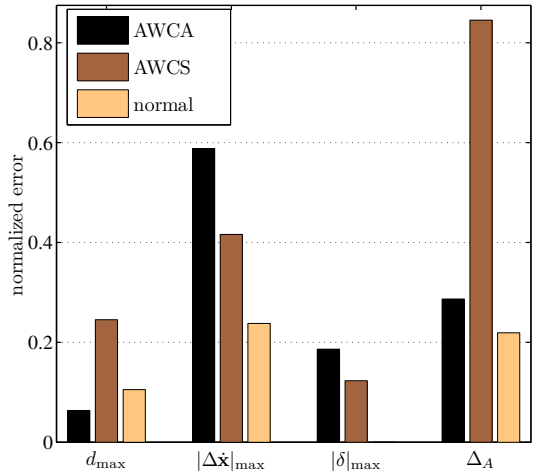

Fig. 14. Comparison of normalized (to the linear control case with saturation) error-values: linear (normal), single-axis anti-windup (AWCS) and multiple-axis anti-windup (AWCA) control.

VI. CONCLUSIONS AND FUTURE WORK

In this paper an anti-windup compensation scheme was presented that ensures trajectory tracking even in case of input saturation. Instead of solving the problem of directionality by using a reference shaping filter, it is tackled by a special parametric design and application of gain scheduling. The design was applied and verified on a planar parallel robot optimized for high-speed operation. Comparison to the non-saturating case as well as to the single-axis anti-windup compensation scheme presented in section V reveals the potential of the holistic approach. Though the contouring error increases in case of input saturation, overshoot and large distortions are avoided – the distortion is kept at a minimum. It just slightly differs from the linear non-saturating case. The transfer of presented control scheme to a computed torque control is not restricted as long as the principle of gain-scheduling is adopted in a similar manner.

The results suggest an extensions to variable boundaries over time of the saturations. An optimized consideration of maximum actuating variable within the linear control-framework by adaption (see eq. (24)) would reduce contouring error and cycle times. Moreover, saturation of multiple axes at the same time is an important point of future work – artificial disturbances and pre-loading of plant controllers are a point when it comes to design of forcing single axis saturation only.

ACKNOWLEDGMENTS

This work was funded by the German Research Foundation (DFG) within the framework of the Collaborative Research Center SFB 562 “Robotic Systems for Handling and Assembly”.

REFERENCES

[1] J.-P. Merlet, *Parallel Robots*, 2nd ed. Netherlands: Kluwer Academics Publishers, 2006.

[2] L. Sciavicco and B. Siciliano, *Modelling and control of robot manipulators*. Springer, Berlin, 2001.

[3] M. Kolbus, T. Reisinger, and J. Maaß, “Robot control based on skill primitives,” in *Proc. of IASTED Conf. on Robotics and Applications*, Cambridge, USA, 2005, pp. 260–266.

[4] B. Finkemeyer, “Robotersteuerungsarchitektur auf Basis von Aktionsprimitiven,” Ph.D. dissertation, TU Braunschweig, 2004, in German.

[5] T. Reisinger, M. Kolbus, and F. Wobbe, “Hybrid position/force-control of a planar parallel robot,” in *Proc. of Conf. on Problems of Automated Electrodrives*, Aluschta, Ukraine, 2005, pp. 250–254.

[6] K.-J. Åström and T. Hägglund, *Automatic Tuning of Pid Controllers*. Instrumentation & Systems, 1988.

[7] J. Öhr, “On anti-windup and control of systems with multiple input saturations: Tools, solutions and case studies,” Ph.D. dissertation, Uppsala University, 2003.

[8] J. C. Doyle, R. S. Smith, and D. F. Enns, “Control of plants with input saturation nonlinearities,” in *Proc. of the 1987 Amer. Contr. Conf.*, Minneapolis, USA, 1987, pp. 1034 – 1039.

[9] P. Hippe, “Windup prevention for stable and unstable mimo systems,” *Intern. J. Syst. Sci.*, vol. 37, no. 2, pp. 67–78, 2006.

[10] L.-W. Tsai, *Robot analysis: the mechanics of serial and parallel manipulators*. USA: John Wiley and Sons, Inc., 1999.

[11] R. M. Murray, Z. Li, and S. S. Sastry, *A mathematical introduction to robotic manipulation*. USA: CRC Press LLC, 1994.

[12] M. W. Spong and M. Vidyasagar, *Robot dynamics and control*. USA: John Wiley and Sons, Inc., 1989.

[13] Y. Nakamura, *Advanced robotics: redundancy and optimization*. Addison-Wesley Publishing Company, 1991.

[14] F. Wobbe, M. Kolbus, and W. Schumacher, “Continuous sliding surfaces versus classical control concepts on parallel robots,” in *Proc. of the 13th IEEE IFAC International Conference on Methods and Models in Automation*, Szczecin, Poland, 2007.

[15] C. Stachera, F. Wobbe, and W. Schumacher, “Jacobian-based derivation of dynamics equations of elastic parallel manipulators,” in *Proc. of the IASTED Asian Conference on Modelling and Simulation (AsiaMS 2007*, Beijing, China, 2007.

[16] B. Dizioglu, *Getriebelehre. Bd. 3. Dynamik*. Vieweg, 1966, in German.

[17] W. Vetter, “Matrix calculus operations and taylor expansions,” *SIAM Review*, vol. 15, pp. 352–369, 1973.

[18] A. Weinmann, *Uncertain models and robust control*. Springer, Wien, 1997.

[19] C. Bohn, “Recursive parameter estimation for nonlinear continuous-time systems through sensitivity-model-based adaptive filters,” Ph.D. dissertation, Ruhr-Universität Bochum, 2000.

[20] O. Föllinger, *Nichtlineare Regelungen I. Grundbegriffe - Anwendung der Zustandsebene - Direkte Methode*, 7th ed. Oldenbourg R., 1998, in German.

[21] W. Leonhard, *Control of Electrical Drives*, 3rd ed. Springer, Berlin, 2001.

[22] C. Brunotte, “Regelung und Identifizierung von Linearmotoren für Werkzeugmaschinen,” Ph.D. dissertation, TU Braunschweig, 1999, in German.

[23] F. Wobbe, W. Böske, and W. Schumacher, “Optimierte Antriebsreglerstrukturen zur Störunterdrückung,” in *SPS/IPC/DRIVES 2006*, Nürnberg, Germany, 2006, pp. 473–482, in German.

[24] F. Wobbe, M. Kolbus, and W. Schumacher, *Automation and Robotics*. InTech Education and Publishing, 2008, ch. Enhanced Motion Control Concepts on Parallel Robots, pp. 17–40.

[25] P. Hippe, *Windup in Control: Its Effects and Their Prevention (Advances in Industrial Control*, 1st ed. Springer, Berlin, 2006.

[26] S. Rönnbäck, K. S. Walgama, and J. Sternby, “An extension to the generalized anti-windup compensator,” in *Proceedings of the 13th IMACS World Congress on Computation and Applied Mathematics*, 1991, pp. 1192–1196.

[27] H.-K. Khalil, *Nonlinear Systems*, 3rd ed. Prentice-Hall, 2001.

[28] J. Raisch, *Mehrgrößenregelung im Frequenzbereich*. Oldenbourg, 1994, in German.

[29] A.-G.-J. MacFarlane and I. Postlethwaite, “The generalised nyquist stability criterion and multivariable root loci,” *Int. J. Control*, vol. 25, pp. 81–127, 1977.

[30] P. Kokotović, H.-K. Khali, and J. O’Reilly, *Singular Perturbation Methods in Control: Analysis and Design (Classics in Applied Mathematics*. Society for Industrial Mathematics, 1987.

[31] K.-J. Åström and B. Wittenmark, *Adaptive Control*, 2nd ed. Pearson, 1995.